Pergamon

Int. J. Solids Structures Vol. 33, No. 25, pp. 3723–3738, 1996

0020-7683/96 $15.00 + .00

0020-7683(95)00206-5

FINITE DEFORMATIONS AND THE DYNAMIC MEASUREMENT OF RADIAL STRAINS IN COMPRESSION KOLSKY BAR EXPERIMENTS

K. T. RAMESH and S. NARASIMHAN
Department of Mechanical Engineering, The Johns Hopkins University, Baltimore, MD, U.S.A.

(*Received* 18 *January* 1995; *in revised form* 22 *August* 1995)

Abstract—A novel technique has been developed for the direct non-contact measurement of the radial deformations of a specimen during a compression Kolsky bar (split-Hopkinson pressure bar) experiment. Application of the new technique makes possible an analysis of the compression Kolsky bar experiment in terms of finite deformations, since the technique provides a complete experimental determination of the deformation gradient tensor during dynamic loading. Using the new technique, we have determined the relative validity of the incompressibility and Bell constraints for finite deformation dynamic plasticity. The experimental results show that the plastic incompressibility constraint is more appropriate for the dynamic compression of 6061-T6 aluminum. It is also shown that the traditional measure of axial strain rate derived from Kolsky bar experiments should be replaced by the axial rate of deformation that is valid for finite deformations. Finally, the technique has been used to investigate the dynamic compression of porous pure iron. It is shown that the new technique extends the capabilities of the compression Kolsky bar technique to include the investigation of plastically compressible materials. Copyright © 1996 Elsevier Science Ltd

1. INTRODUCTION AND BACKGROUND

The compression Kolsky bar or split-Hopkinson pressure bar (SHPB) has become the most widely used experimental technique for the determination of the mechanical properties of materials at intermediate strain rates (10^2–10^4 s^{-1}). The technique was first developed by Kolsky (1949), and has since been used to study the dynamic behavior of metals, polymers, ceramics, and composites. An excellent review of the experimental technique is provided by Follansbee (1985).

However, the range of application of the compression Kolsky bar is limited in several ways. The primary limitations arise from the fact that the technique makes measurements at significant distances from the specimen, and then uses the elasticity of the bars and assumptions on the interface conditions to deduce the properties of the material under study. Since longitudinal waves undergo dispersion in bars, and since the interface conditions are difficult to quantify, there is usually some uncertainty as to the strain rate and the strain in the specimen. The limitations placed on the experimental technique in terms of frictional constraints, radial inertia and so forth result in restrictions on specimen sizes, length-to-diameter ratios and surface preparation for a valid test [e.g. Bertholf and Karnes (1975)]. When the experiments are correctly designed using these now well-established restrictions, direct measurement of local strains on the sample using strain gages has shown that the signals obtained from the remote gages on the bars provide quite accurate results for specimen strains greater than about 1% [e.g. Sharpe and Hoge (1972)].

Very small strains are developed in relatively brittle materials such as ceramics and composites, and so strain gages on the specimen are often required in experiments on these materials. Indeed, several researchers who study ceramics and composites routinely apply strain gages directly to the specimen [e.g. Staehler *et al.* (1993), Subhash and Nemat-Nasser (1993), Ramesh and Ravichandran (1990)]. However, the application of strain gages directly on each small specimen is a comparatively expensive and time-consuming process. A direct non-contact measure of the specimen strain would be of great value under these circumstances.

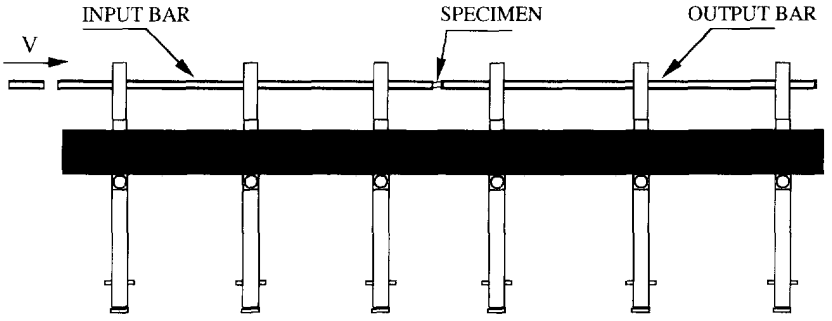

Fig. 1. Schematic of the compression Kolsky bar (or split-Hopkinson pressure bar).

This paper represents a major extension of the range of application of the compression Kolsky bar, utilizing a finite deformation analysis that is made possible because of a novel experimental technique that we have developed. The new technique allows the direct non-contact measurement of radial strains in the specimen during a compression Kolsky bar test. If one assumes plastic incompressibility, then this new technique provides a direct measure of the specimen strain and strain rate.

For the sake of completeness, and because the new technique represents a substantial extension, we begin with a very brief description of the traditional compression Kolsky bar technique. We then proceed to describe the new experimental technique in detail, and use the results to formulate the finite deformation kinematics corresponding to the experiment. When applied to the dynamic plastic deformation of metals, the finite deformation analysis coupled with the experimental measurements allows us to examine experimentally the incompressibility constraint that is commonly assumed in plasticity. When applied to the plastic deformation of porous metals, the technique allows us to extract the first complete experimental measurements of the plastic compressibility of metals during dynamic deformations.

The compression Kolsky bar (or SHPB)

The compression Kolsky bar or split-Hopkinson pressure bar (Fig. 1) consists of two long metal bars that are designed to remain elastic throughout the test. These bars sandwich a short cylindrical specimen. One end of one of the bars (the incident or input bar) is impacted by a projectile (typically fired from a gas gun). The compressive pulse generated by the impact propagates down the incident bar into the specimen. After several reverberations within the specimen, a transmitted pulse is sent into the second bar (called the transmitter or output bar) and a reflected pulse is sent back into the incident bar. Conventionally, strain gages placed on the input and output bars are used to measure the pulses propagating in the bars.

Let the strain in the reflected pulse be denoted by ε_R and that in the transmitted pulse by ε_T. Then, once a uniform stress state has been achieved in the specimen, we obtain expressions for the mean specimen stress S and the specimen strain e_s in terms of the strains in the reflected and transmitted pulses [e.g. Lindholm (1964)]:

$$S = \frac{EA_b}{A_s}\varepsilon_T \tag{1}$$

and

$$e_s = \frac{u_1 - u_2}{l_0} = \frac{2c_0}{l_0}\int_0^t \varepsilon_R \, \mathrm{d}t \tag{2}$$

where l_0 and A_s are the specimen initial length and specimen initial cross-sectional area, A_b is the bar cross-section area, and u_1 and u_2 are the displacements corresponding to the specimen-input bar and specimen-output bar interfaces respectively. Note that e_s is usually

defined as $(l_0-l)/l_0$ so that it is positive for compressive deformations (l is the current specimen length). The mean specimen strain rate is then given by

$$\dot{e}_s = \frac{2c_0}{l_0}\varepsilon_R \tag{3}$$

Here c_0 is the bar velocity, given by $\sqrt{E/\rho}$; E is the Young's modulus, and ρ is the mass density of the bar material. Thus the strain rate in the specimen can be determined from the reflected pulse, and the stress in the specimen can be determined from the transmitted pulse. Typically the strain gage signals are processed to correct for the dispersion of the longitudinal wave that occurs in the bars (note that all of the remote gage results presented in this paper have been corrected for dispersion). The corrected strain rate pulse is then integrated and the resulting strain-time history correlated with the stress-time history to obtain the engineering stress-strain curve at each strain rate (corresponding to that in (3)).

Note that the relations (2) and (3) were obtained after assuming the equilibration of the stress state throughout the specimen, a process that takes some time and during which some (small) strain is developed within the specimen. For relatively brittle materials, such as ceramics, most of the material behavior of interest may occur during those small initial strains; hence the use of strain gages attached directly to the specimen for such experiments [e.g. Staehler *et al.* (1993), Ramesh and Ravichandran (1990)].

The compression Kolsky bar technique assumes that the specimen remains in a uniaxial stress state, so that the measurement of the axial stress (through the measurement of the transmitted load) is sufficient to completely characterize the stress state. This is likely a good approximation, considering the specimen dimensions used in practice, and assuming properly lubricated specimen-bar interfaces (for a detailed discussion of these issues, see the papers by Bertholf and Karnes (1975) and by Jahsman (1971)). However, assuming homogeneous axisymmetric deformations only for the specimen, it is clear that both axial and radial strains are developed in the specimen during the experiment. Yet the compression Kolsky bar technique provides a measure of only the axial strain in the specimen (through (2)). One is therefore forced to assume incompressibility of the material of the specimen in order to obtain an estimate of the radial strain. Further, the assumption of material incompressibility is required in order to obtain true stress-true strain data from such experiments.

The next section presents a new technique for the direct, non-contact measurement of the radial strain of the specimen during the dynamic deformation. Thus the constraint of incompressibility need no longer be imposed in order to use the compression Kolsky bar (this would be of particular value when studying porous metals and geologic materials).

2. THE NEW EXPERIMENTAL TECHNIQUE

The Laser Occlusive Radius Detector

A schematic diagram of the experimental configuration for the Laser Occlusive Radius Detector (LORD) is shown in Fig. 2. The LORD system is set up so that its operational

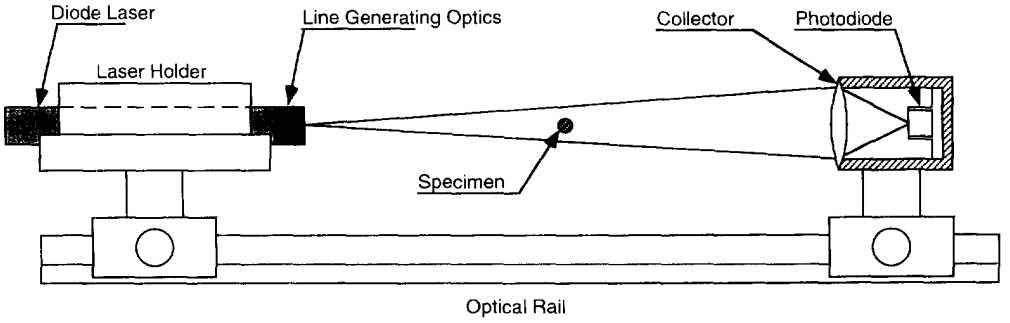

Fig. 2. Schematic of the experimental configuration of the Laser Occlusive Radius Detector (LORD).

plane is orthogonal to the axis of the compression Kolsky bar, with the Kolsky bar specimen alone intersecting that plane. The system consists of three major components: an optical arrangement for generating a laser sheet, optics and optoelectronics for collecting the light, and the necessary mounting systems. A photograph of the current incarnation of the LORD is presented in Fig. 3. Part of the Kolsky bar can also be seen in the photograph.

The optical emission system consists of a diode laser operating at 670 nm and generating 3 mW of output power, integrated with focusing and line generating optics that produce a sheet of laser light with a central region of nearly uniform intensity per unit length across the sheet. The laser is mounted within a specially designed holder to improve pointing stability, and the entire arrangement is mounted on an optical rail for ease of alignment. The integrated optics produces a sheet of coherent light that can be focused to a thickness of a fraction of a millimeter at the specimen. The sheet is emitted with a fixed divergence angle in the plane of the sheet (which is orthogonal to the specimen axis); this can be collimated to generate a parallel beam in the plane, but such collimation is not necessary.

The sensing system consists of a collector lens that integrates all of the incoming light to a silicon PIN photodiode located at its focus. The photodiode signal is pre-amplified; the optoelectronics and the preamplifier together have a bandwidth of 50 MHz. The output of this system consists of a voltage that is proportional to the total amount of light entering the collector lens.

Principle of operation

The basic principle of operation of the LORD is extremely simple. The specimen blocks part of the laser sheet before it reaches the collection optics; as the specimen is deformed, its diameter increases, and it occludes increasing amounts of light in the sheet, resulting in a drop in the voltage output from the photodiode. By capturing the photodiode signal during the test, and using a calibration to relate the voltage output to the diametral change, we are able to extract the dynamic radial deformations that are developed in the specimen during a compression Kolsky bar test.

The LORD system is calibrated by using a conical calibration specimen that is slowly translated (along the cone axis) into the laser sheet while monitoring the LORD output. Since the cone angle is known, this procedure provides an output voltage versus specimen diameter calibration curve such as that shown in Fig. 4. Note the linearity of the curve (representing the uniformity of the laser intensity within the sheet). An aperture stop was used to eliminate the edges of the sheet, which contain the maximum variation in the intensity. Specimen radial strain can then be directly obtained from the dynamic tests using the calibration curve of Fig. 4.

Figure 5 presents an example of the output of the LORD, obtained during a dynamic compression test on 6061-T6 aluminum at a nominal strain rate of $3.8 \times 10^3\ s^{-1}$. The signal has been smoothed to remove digital noise (introduced by the vertical resolution of the digitizing oscilloscope), but has not been otherwise processed; the raw data from the digitizer is superimposed on the smoothed curve for purposes of comparison. The initial output level represents the total light intensity incident on the collector before specimen deformation begins (i.e. it represents the initial diameter), and the final output level represents the final specimen diameter. The diametral change in this case was 0.488 mm. Note, however, that the output of the detector does not represent the diameter of a fixed station along the specimen axis. The rigid body translation inherent in the Kolsky bar experiment causes the detector to sample different parts of the specimen as time increases, and thus interpretation of the signal requires the assumption of translational symmetry of the deformations along the specimen axis. During very early times, when waves are still reverberating within the specimen, the detector output represents an average diameter within the sampling time (40 ns) of the digitizer. The instrumentation in the current incarnation of the LORD does not permit the resolution of the wave motion itself, both in terms of the temporal resolution of the oscilloscope and in terms of the accurate measurement of the small diametral changes associated with each wave.

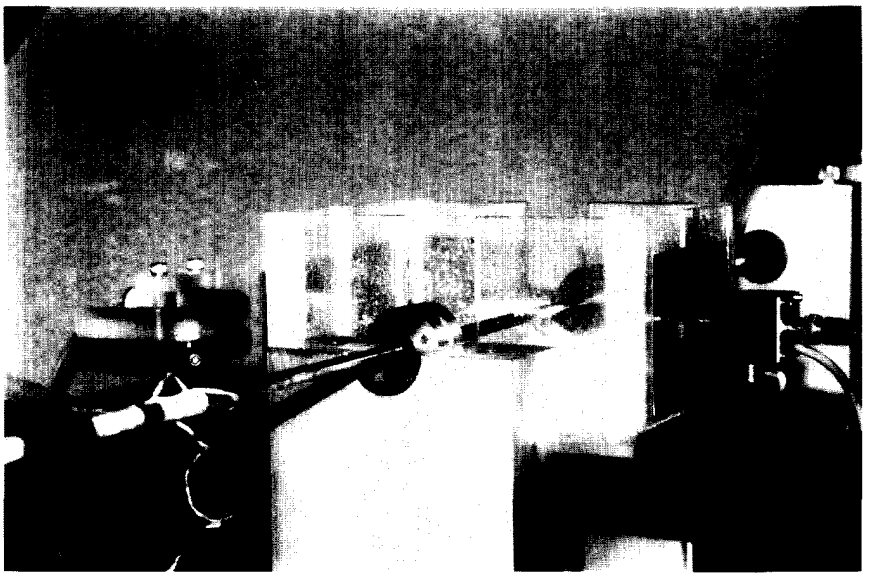

Fig. 3. Photograph of the Laser Occlusive Radius Detector system.

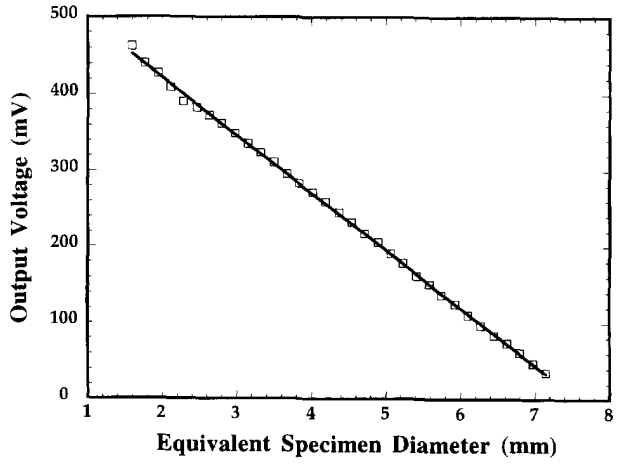

Fig. 4. Calibration curve for the LORD using a conical calibration specimen.

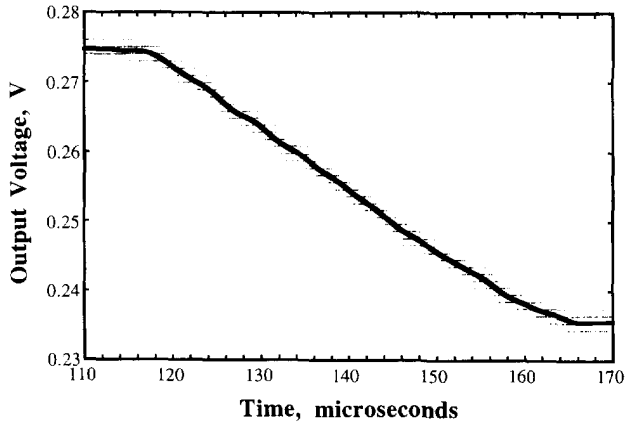

Fig. 5. Typical output from the LORD system: test on a 6061-T6 aluminum sample.

The next section discusses the kinematics of finite deformations within compression Kolsky bar experiments and provides the theoretical framework within which the results of the new experimental technique can be discussed.

Finite deformation kinematics for Kolsky bar experiments

Consider the finite compression of a cylindrical Kolsky bar specimen of initial length l_0 and initial diameter $2R$ (Fig. 6). For simplicity, let us assume that the deformations are axisymmetric and always homogeneous (in particular, we shall ignore the wave propagation within the specimen, and we shall assume sufficiently lubricated bar-specimen interfaces). Defining the Cartesian coordinate system shown in Fig. 6, we can describe the finite deformations of the specimen through the relations

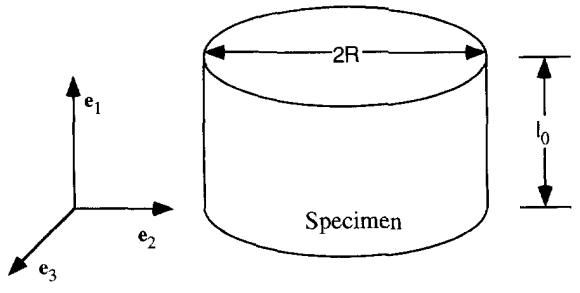

Fig. 6. Schematic diagram of specimen and coordinate system for analysis.

$$x_1 = \lambda(t)X_1$$
$$x_2 = \omega(t)X_2$$
$$x_3 = \omega(t)X_3 \tag{4}$$

where the x_i represent the current coordinates of a material particle initially at the coordinates X_i. The quantities $\lambda(t)$ and $\omega(t)$ are the axial and radial stretches respectively:

$$\lambda(t) = \frac{l(t)}{l_0} \tag{5}$$

and

$$\omega(t) = \frac{r(t)}{R}, \tag{6}$$

where $l(t)$ and $r(t)$ are the current length and the current radius. The deformation gradient corresponding to eqn (4) is given by

$$\mathbf{F} = \lambda(t)\mathbf{e}_1\mathbf{e}_1 + \omega(t)(\mathbf{e}_2\mathbf{e}_2 + \mathbf{e}_3\mathbf{e}_3) \tag{7}$$

where the $\mathbf{e}_i$ represent unit vectors along the coordinate axes x_i, and the notation $\mathbf{e}_i\mathbf{e}_j$ represents the tensor product $\mathbf{e}_i \otimes \mathbf{e}_j$. For a full elastic-plastic analysis we would assume that the total deformation gradient can be multiplicatively decomposed into elastic and plastic parts:

$$\mathbf{F} = \mathbf{F}^e\mathbf{F}^p. \tag{8}$$

Further, the intermediate configuration can be chosen without rotation so that the plastic deformation gradient can be defined as the symmetric tensor

$$\mathbf{F}^p = \lambda_p(t)\mathbf{e}_1\mathbf{e}_1 + \omega_p(t)(\mathbf{e}_2\mathbf{e}_2 + \mathbf{e}_3\mathbf{e}_3) \tag{9}$$

where $\lambda_p(t)$ and $\omega_p(t)$ are plastic stretch ratio. Equation (8) can then be solved for the elastic deformation gradient:

$$\mathbf{F}^e = \frac{\lambda}{\lambda_p}\mathbf{e}_1\mathbf{e}_1 + \frac{\omega}{\omega_p}(\mathbf{e}_2\mathbf{e}_2 + \mathbf{e}_3\mathbf{e}_3). \tag{10}$$

However, the elastic deformations are extremely small in comparison to the plastic deformations that are developed within Kolsky bar experiments. Thus, an excellent approximation to the kinematics is obtained by setting the plastic deformation gradient identically equal to the total deformation gradient, so that

$$\mathbf{F}^p = \mathbf{F} = \lambda(t)\mathbf{e}_1\mathbf{e}_1 + \omega(t)(\mathbf{e}_2\mathbf{e}_2 + \mathbf{e}_3\mathbf{e}_3). \tag{11}$$

Independent measurements of the stretches in eqns (5–6) then completely determine the deformations in the problem. Of course, the axial and radial stretches may not be independent variables. For example, a common assumption in plasticity is that plastic deformations are incompressible, corresponding to the constraint that

$$J = \det \mathbf{F} = \lambda\omega^2 = 1. \tag{12}$$

The incompressibility constraint of eqn (12) is usually invoked in the analysis of

Kolsky bar experiments to convert the measured engineering stresses to true stresses. An alternative constraint that has sometimes been invoked is championed by Bell [e.g. Bell (1985)], and amounts to the requirement that

$$\text{tr}\,\mathbf{V} = \text{tr}\sqrt{\mathbf{F}\mathbf{F}^T} = \lambda + 2\omega = 3 \tag{13}$$

where the notation "tr" represents the trace operator, and $\mathbf{V}$ is the left stretch tensor corresponding to the deformation gradient in eqn (11). Independent measurements of the stretches λ and ω during the dynamic compression would provide the opportunity to distinguish between the incompressibility (eqn. 12) and Bell (eqn. 13) constraints for any given material and deformation regime.

The output of the LORD system provides the radial stretch directly, since it measures the specimen radius as a function of time during the compression. The axial stretch can be obtained from the reflected pulse in the bar, using the relation [e.g. Ramesh (1991)]

$$\lambda(t) = 1 - \frac{2c_0}{l_0}\int_0^t \varepsilon_R(\tau)\,\mathrm{d}\tau. \tag{14}$$

Thus we are now able to experimentally determine the entire deformation gradient tensor (for an isotropic material undergoing axisymmetric deformations). The measured stretches can then be used to check the validity of proposed constraints such as incompressibility, and to make the Kolsky bar technique useful even for the study of materials for which the constraints are not established (e.g. porous materials).

The rate of deformation tensor $\mathbf{D}$ for this uniaxial compression problem is identical to the velocity gradient (since the deformation gradient is symmetric) and is given by

$$\mathbf{D}^p = \mathbf{D} = \mathbf{L} = \frac{\dot{\lambda}}{\lambda}\mathbf{e}_1\mathbf{e}_1 + \frac{\dot{\omega}}{\omega}(\mathbf{e}_2\mathbf{e}_2 + \mathbf{e}_3\mathbf{e}_3) \tag{15}$$

where $\dot{\lambda}$ and $\dot{\omega}$ are the material time derivatives of the axial and radial stretches, respectively. It should be pointed out here that in the past, although the results of compression Kolsky bar experiments have usually been presented in terms of true stresses and true strains, the axial strain rates quoted have always been the nominal strain rate ($\dot{l}/l_0$) rather than the true axial rate of deformation ($\dot{\lambda}/\lambda$). A more consistent finite deformation approach is clearly of value for the development of accurate constitutive models.

The next section presents some results obtained using the LORD on fully dense metals (where plastic incompressibility is usually assumed to be a good approximation) and on porous metals (which are plastically compressible). The application of the finite deformation kinematics to the interpretation of experimental data is also demonstrated.

Results and discussion

Dynamic compression of 6061-*T6 Al.* We begin by discussing the results of a typical experiment on the dynamic compression of 6061-T6 aluminum alloy. The initial specimen diameter was 4.762 mm, and the initial specimen length was 2.722 mm. A summary of the experimental results on the dynamic properties of this material is presented in the work of Yadav *et al.* (1994). We focus here on the application of the LORD system to these otherwise standard compression Kolsky bar experiments.

The LORD output shown in Fig. 5 was obtained during the dynamic compression of 6061-T6 Al at a nominal axial strain rate of $3.9 \times 10^3\ \text{s}^{-1}$, and can be converted into radius information using the calibration curve from Fig. 4. The radial stretch $\omega(t)$ can then be computed as the ratio of the current radius $r(t)$ to the initial specimen radius R using eqn

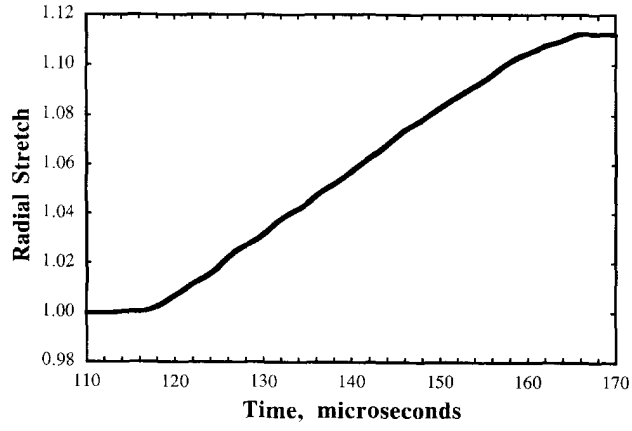

Fig. 7. Radial stretch measured using the LORD system for the 6061-T6 aluminum test result presented in Fig. 5.

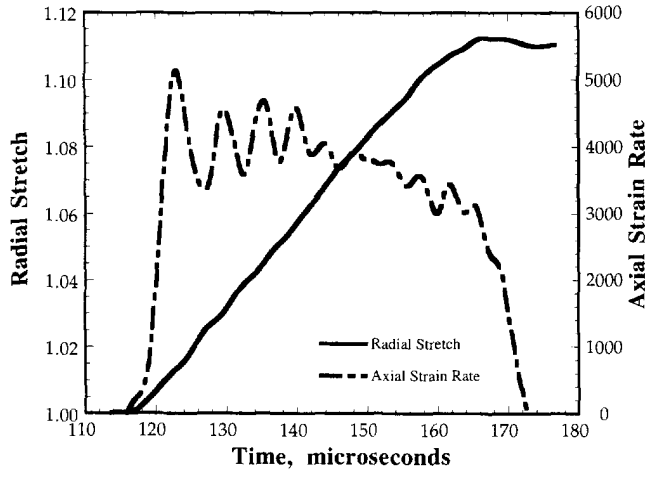

Fig. 8. Comparison of the output of the LORD system, presented as radial stretch versus time, with the axial strain rate history computed from the reflected strain pulse (measured using strain gages on the bar). Note that there is very little change in radius once the strain rate pulse begins to unload.

(6). The corresponding history of the radial stretch is presented in Fig. 7. The total radial change is 0.244 mm. Note that this measurement of the radial stretch is a direct measure; stress equilibration need not be invoked to compute it, in contrast to the axial strains computed using eqn (2). A radial stretch rate $\dot{\omega}/\omega$ can be computed from the slope of the curve in Fig. 7, analogous to the axial strain rate computed using eqn (3). In interpreting Fig. 7, it is important to note that the vertical resolution (8-bits) of the digitizing oscilloscope was such that radial changes smaller than 5 μm could not be resolved; thus the elastic deformations are lost in the digital noise.

We now have two experimental measurements (axial and radial) of the deformation in the specimen. The two measurements are both presented in Fig. 8, using a common time base in which time zero corresponds to the arrival of the incident pulse at the strain gage on the incident bar (this pulse is used as a common trigger signal for both data acquisition systems). The axial information presented in Fig. 8 is the reflected pulse (normalized using eqn (3) to obtain the axial strain rate). This reflected pulse has been corrected for dispersion back to the time and position at which the pulse is at the specimen itself (the initial blip observed in this reflected pulse before the primary rise does not represent a mechanical signal; it results from a short electrical noise spike generated when the pulse arrives at the lead wire connections for the strain gages). The radial information presented in Fig. 8 is the radial stretch of Fig. 7. Note that the radial deformations begin at approximately the time at which the axial strain rate pulse begins its rise. The section of the radial stretch

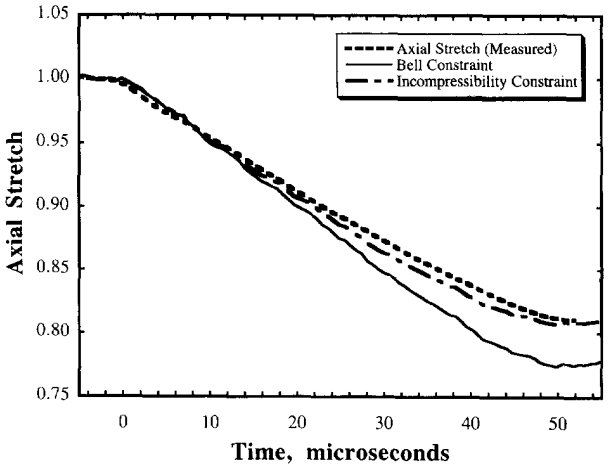

Fig. 9. Comparison of the axial stretch measured using the strain gages on the bars and that computed using the radial stretch measured by the LORD system using the incompressibility constraint (eqn 12) and the Bell constraint (eqn 13).

curve during the risetime of the axial pulse is somewhat different from the rest of the radial stretch curve, because during this time waves are still reverberating within the specimen and a homogeneous deformation has not been established. The radial strain increases relatively uniformly after the initial risetime until the reflected pulse begins to unload, corresponding to a reduction in the rate of deformation in the specimen. The radial deformations are small once unloading begins; this observation may be explained by assuming that the unloading is largely elastic (for this material), with reverberations of the unloading waves occurring within the specimen. A consequence of the small radial deformations after unloading is that the apparent duration of the radial stretch is slightly smaller than the apparent duration of the axial strain rate pulse.

Integration of the reflected pulse using eqn (14) provides the axial stretch in the specimen. This experimental measurement of the axial stretch can be compared directly with the axial stretch computed from the measured radial stretch using either the plastic incompressibility constraint (eqn 12) or the Bell constraint (eqn 13). Such a comparison is presented in Fig. 9. It is clear that the plastic incompressibility constraint is more in accord with the measured axial and radial stretches. Note that this measure of the constraint is obtained from time-resolved measurements of the full deformation gradient tensor during the dynamic deformation of this material, rather than merely from measurement of the geometry before and after plastic deformation. Thus elastic unloading is not an issue in this evaluation of the plasticity constraint. Note further that the plastic deformations that are developed in these experiments are indeed finite, and are sufficient to resolve differences between the two constraints.

Since plastic incompressibility has been determined to be the appropriate constraint for the finite plastic deformations of this material, we will use it in our further discussions of the results on 6061-T6 aluminum. The incompressibility constraint can be used in conjunction with the radial stretch measured with the LORD system to provide the axial strain in the specimen, from data measured directly at the specimen. The stress in the specimen can be obtained from eqn (1) using the transmitted pulse. The true stress σ and the engineering stress S from eqn (1) are related very simply by

$$\sigma a = SA \tag{16}$$

where A and a are the initial and current cross-section areas respectively. In the general case, it follows that the true stress can then be obtained from the relation

$$\sigma = S\frac{A}{a} = S\frac{1}{J}\frac{l}{l_0} = S\frac{\lambda}{J}. \tag{17}$$

In the particular case of axisymmetric deformations, eqn (17) reduces to

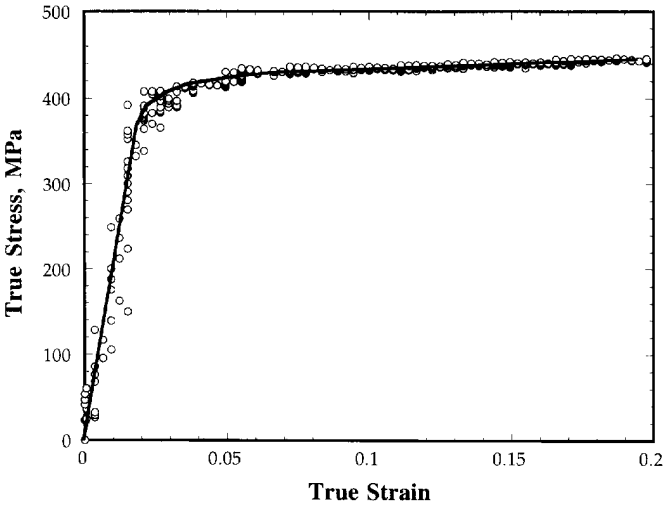

Fig. 10. Stress-strain curve obtained for 6061-T6 aluminum using the radial stretch data of Fig. 7 and the incompressibility constraint.

$$\sigma = \frac{S}{\omega^2}. \tag{18}$$

This result could of course be directly obtained also from the first part of eqn (17) in terms of the area ratio. Thus eqn (18) and the direct measurement of the radial stretch provides the true stress directly from the engineering stress. Note that eqn (18) is correct whether or not the material is plastically incompressible.

Using eqn (18) and the measured radial stretch, a true stress-true strain curve can be obtained for the specimen material (the true strain measure used is $\varepsilon = \ln(l/l_0) = \ln \lambda$). Note that this procedure does not use any information from the incident or reflected pulses, suggesting that we could do away with the incident bar altogether (we shall discuss this approach subsequently). The true stress-true strain curve obtained in this way for the 6061-T6 aluminum (using the LORD data of Fig. 8) is presented in Fig. 10.

The constitutive information in Fig. 10 is presented in terms of true stress and true strain; what is the corresponding strain rate? Using plastic incompressibility, we have

$$\det \mathbf{F}^p = \det \mathbf{F} = 1, \Rightarrow \operatorname{tr} \mathbf{D}^p = 0. \tag{19}$$

Using eqn (15) together with eqn (19), we obtain

$$\frac{\dot{\lambda}}{\lambda} + 2\frac{\dot{\omega}}{\omega} = 0. \tag{20}$$

Thus for incompressible materials the axial rate of deformation can be computed from the radial rate of deformation, which can be obtained directly from the measured time-history of the radial deformations. Note that no dispersion correction is necessary to obtain the axial rate of deformation using this approach, since the radial deformations are measured directly at the specimen. It should be emphasized that all of the remote gage results presented in this paper have been corrected for the dispersion of longitudinal waves propagating in the first mode in the bars.

The discussion of the previous paragraphs brings up an issue that is extremely important for the constitutive characterization of materials at high strain rates. Almost uniformly in the literature, the axial "true strains" quoted are logarithmic strains obtained using eqn (2) and the relation $\varepsilon = \ln(l/l_0) = \ln(1 - e_s)$; and the "true stresses" quoted are obtained using eqns (1) and (17) and invoking incompressibility: $\sigma_s = S(l/l_0) = S(1 - e_s)$. However, the strain rates quoted for compression Kolsky bar experiments are always obtained using

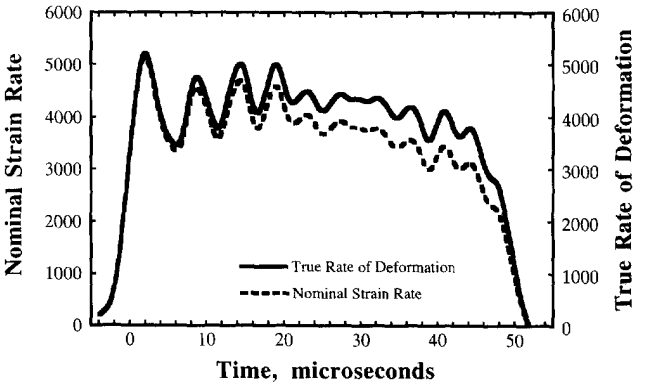

Fig. 11. Comparison of the nominal axial strain rate with the true axial rate of deformation for the test on 6061-T6 aluminum presented in Fig. 10.

eqn (3), and represent the nominal strain rate $\dot{l}/l_0$ rather than the true axial rate of deformation $\dot{l}/l = \dot{\lambda}/\lambda$. For the purposes of constitutive modeling it is important to be consistent in the choice of configuration, so that Kolsky bar strain rate data should really be quoted in terms of the true axial rate of deformation $\dot{\varepsilon} = \dot{l}/l = \dot{\lambda}/\lambda$. This is actually very easy to do, even without the use of the LORD system, since we have

$$\dot{\varepsilon} = \frac{\dot{\lambda}}{\lambda} = \frac{\dot{l}}{l} = \frac{\dot{l}}{l_0}\frac{l_0}{l} = \frac{\dot{e}_s}{(1-e_s)}. \tag{21}$$

There is a substantial difference between the nominal strain rate and the rate of deformation for the finite deformations that are developed in compression Kolsky bar experiments. For example, Fig. 11 presents a comparison of the nominal axial strain rate with the axial rate of deformation for the experiment on 6061-T6 aluminum corresponding to Fig. 10. It is clear that the mean rate of deformation ($4.3 \times 10^3\ s^{-1}$) is significantly higher than the mean nominal axial strain rate ($3.9 \times 10^3\ s^{-1}$); further, the variation in the rate of deformation is smaller than that in the nominal rate. The use of the rate of deformation results in a significant upward revision of the quoted strain rate corresponding to a given Kolsky bar experiment, and may have significant effects on the rate-sensitivities that are estimated for materials. Another consequence of using the rate of deformation is that there is less of a reduction of the rate with increasing time during an experiment. This is an important effect, because most high-rate laboratories use wave-shaping of the incident pulse in order to obtain a nominal strain rate that is more nearly constant during a test (especially for work-hardening materials).

One critical result of using the procedures leading up to eqn (20) to obtain the stress-strain curve is that no information is required from the incident bar, while the output bar is now used solely as a force transducer. A direct extension of this idea is to use the LORD system to measure radial deformations on a specimen that is directly impacted by the projectile, with the specimen backed by an output bar. The advantage of this approach is that somewhat higher strain rates can be achieved in the specimen while still accounting for the usual concerns of radial inertia and frictional end conditions. Such a direct impact high strain rate setup is currently under construction. A version of this approach has been implemented by Gorham *et al.*, who used a high-speed framing camera to record the specimen deformations during direct impact. However, the LORD system is dramatically cheaper to implement and much more accurate in terms of temporal and spatial resolution. Another version of this direct impact high strain rate experiment was used by Dharan and Hauser (1970); lacking a direct measure of strain, these authors were required to make very restrictive assumptions on the deformations in order to interpret their experiments.

The experimental technique used here is extremely easily adapted to the simultaneous local measurement of axial and radial strains, using two orthogonal line lasers (one measuring the distance between the bar faces, and the other measuring the specimen diameter).

A paper describing such a measurement system is under preparation (Ramesh and Garmon, 1995). For the case where axisymmetric deformations cannot be guaranteed, as with anisotropic materials, three orthogonal line lasers can be used (i.e., the three stretches in the $\mathbf{e}_1$, $\mathbf{e}_2$ and $\mathbf{e}_3$ directions can be independently measured). However, our experiments to date have focused on isotropic materials.

In the next section we present the application of the LORD system to investigation of the dynamic compression of porous metals (in which plastic compressibility is certain). Note that the investigation of porous metals within the compression Kolsky bar requires a measure of the radial deformations, since plastic incompressibility can no longer be used to compute the total deformations or to reduce the engineering stresses to true stresses.

Dynamic compression of a porous metal

The characterization of porous metals at high strain rates is essential for the accurate modeling of manufacturing processes involving powder precursors (e.g. the high-speed forging of a powder metal component). Since a large number of the manufacturing processes devoted to powder metal parts involve overall compressive stresses (e.g. forging and extrusion), the dynamic compressive behavior of porous metals is of particular interest. The fundamental approach presented here involves the characterization of the porous metal in terms of the overall dynamic behavior, accounting for the evolution of the porosity in a volume-averaged sense but without attempting to track individual pores.

The results presented here were obtained on porous pure iron. The porous iron was produced by CIPing Hoeganaes Ancorsteel 1000 powders, which are 99.75% pure iron, with C < 0.03%, S < 0.025%, Mn < 0.25%, and Cu < 0.3%. Porous iron compacts were made by CIPing, then sintered in hydrogen at 1200°C for 20 hours and furnace cooled. Compression Kolsky bar specimens were machined out of the sintered compact using EDM, and then annealed at 800°C for one hour in a hydrogen atmosphere. The results presented in this paper are for a pore volume fraction of 13.6%. A much more detailed description of the experiments is presented by da Silva and Ramesh (1995).

Just as with the fully dense 6061-T6 material, the LORD system was used to measure the radial stretch $\omega(t)$ during the dynamic compression of the porous iron. The axial stretch $\lambda(t)$ was computed from the strain gage signals in the input bar using eqn (14). These two independent measures of the deformation completely define the deformation gradient $\mathbf{F}$, and so the volume ratio can be computed from the relation

$$J = \det \mathbf{F} = \lambda \omega^2. \tag{22}$$

Since the elastic deformations are negligible in comparison to the plastic deformations, this volume ratio represents the overall plastic compressibility of the porous metal. If it is now assumed that the iron matrix itself is plastically incompressible, eqn (22) leads to a measure of the evolution of the pore volume fraction. Detailed results on the evolution of the porosity during compressive deformations are presented by da Silva and Ramesh (1995).

With the complete kinematics of the deformation known from the experiment, it is now possible to represent the overall behavior of the porous iron in terms of a true stress–true strain curve (note that the true stress must now be calculated taking the evolving volume of the specimen into account). Equation (18) and the direct measurement of the radial stretch provides the true stress directly from the nominal stress. Since the material is plastically compressible, there is no means (note eqn (17)) of obtaining the true stress without this measure of the radial deformations. For example, the true stress versus true strain curve obtained during a dynamic compression test on porous iron is presented in Fig. 12. The axial rate of deformation corresponding to the stress-strain curve of Fig. 12 is $3.9 \times 10^3\ \mathrm{s}^{-1}$.

Conclusions

An analysis of the compression Kolsky bar experiment in terms of finite deformations has been developed, utilizing the results of a novel technique for the direct non-contact

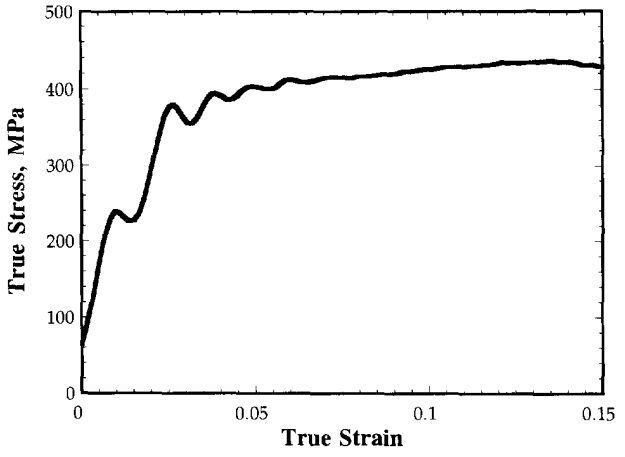

Fig. 12. Example of a true stress-true strain curve obtained during the dynamic compression of porous pure iron.

measurement of the radial deformations of a specimen during a compression Kolsky bar experiment. Using the finite deformation analysis in conjunction with the new technique, we have examined the relative validity of the incompressibility and Bell constraints for finite deformation dynamic plasticity. The experimental results show that the plastic incompressibility constraint is more appropriate for the dynamic compression of 6061-T6 aluminum. Further, it has been shown that the traditional measure of axial strain rate in Kolsky bar experiments should be replaced by a measure of the axial rate of deformation. Finally, the technique has been used to investigate the plastic deformations of porous iron during dynamic compressive loading. Thus the enhancement of the traditional compression Kolsky bar technique with the LORD system makes it possible to also investigate the high-strain rate behavior of plastically compressible materials. However, the difficulties associated with the development of accurately characterized large-strain experiments that operate at a constant high rate must still be carefully addressed.

Acknowledgments—The research described in this paper was supported in part by the U.S. Army Research Office through Award No. DAAL0391G0079 to K. T. Ramesh; this research support is gratefully acknowledged. The authors also wish to thank M. da Silva and D. R. Chichili for help with the experiments.

REFERENCES

Bell, J. F. (1985). Contemporary perspectives in finite strain plasticity. *Int. J. Plast.* **1**, 3–27.

Bertholf, L. D. and Karnes, C. H. (1975). Two-dimensional analysis of the split-Hopkinson pressure bar system. *J. Mech. Phys. Sol.* **23**, 1–19.

da Silva, M. and Ramesh, K. T. (1995). The effect of porosity and porosity evolution on the dynamic compressive deformations of metals. In preparation.

Dharan, C. K. H. and Hauser, F. E. (1970). Determination of stress-strain characteristics at very high strain rates. *Experimental Mech.* **10**, 370–376.

Follansbee, P. S. (1985). The Hopkinson bar. In *ASM Metals Handbook*: Vol. 8, ASM International, Materials Park, OH, pp. 198–203.

Gorham, D. A., Pope, P. H. and Field, J. E. (1992). An improved method for compressive stress-strain measurements at very high strain rates. *Proc. R. Soc. Lond.* **A 438**, 153–170.

Jahsman, W. E. (1971). Re-examination of the Kolsky technique for measuring dynamic material behavior. *J. Appl. Mech.*, 75–82.

Kolsky, H. (1949). An investigation of the mechanical properties of materials at very high rates of loading. *Proc. Phys. Soc. Lond.* **B 62**, 676–682.

Lindholm, U. S. (1964). Some experiments with the split-Hopkinson pressure bar. *J. Mech. Phys. Sol.* **12**, 317–335.

Ramesh, K. T. (1991). The short-time compressibility of elastohydrodynamic lubricants. *J. Tribology* **113**, 361–371.

Ramesh, K. T. and Garmon, J. (1995). An optical technique for the simultaneous measurement of axial and radial stretches in the compression Kolsky bar. In preparation.

Ramesh, K. T. and Ravichandran, G. (1993). Dynamic behavior of a boron-carbide-aluminum cermet: experiments and observations. *Mech. Mat.* **10**, 19–29.

Sharpe, W. N., Jr. and Hoge, K. G. (1972) Specimen strain measurement in the split-Hopkinson-pressure-bar experiment. *Exp. Mech.* **12**, 570–574.

Staehler, J. M., Predebon, W. W., Pletka, B. J., and Lankford, J. (1993). Testing of high-strength ceramics with the split-Hopkinson pressure bar. *J. Am. Cer. Soc.* **76,** 536–538.

Subhash, G. and Nemat-Nasser, S. (1993). Dynamic stress induced transformation and texture formation in uniaxial compression of zirconia ceramics. *J. Am. Cer. Soc.* **76,** 153–165.

Yadav, S., Chichili, D. R. and Ramesh, K. T. (1995). The mechanical response of a 6061–T6 Al/Al_2O_3 metal-matrix composite at high rates of deformation. *Acta Met. Mat.*, in press.